

Static and fluctuating zigzag order, and possible signatures of Kitaev physics, in torque measurements of α -RuCl₃

S. Froude-Powers, Subin Kim, Jacob Gordon, Hae-Young Kee, Young-June Kim, and S.R. Julian*

Department of Physics, University of Toronto, Toronto, Ontario, M5S 1A7 Canada

(Dated: December 23, 2023)

We have measured magnetic torque on a $T_N = 7$ K single crystal of α -RuCl₃, as a function of the field angle in the ab -plane, focusing on temperatures between 2 and 20 K and fields from 0 to 9 T. We find a rich spectrum of signals, many of which can be classified by their angular periodicity. The sample shows an oscillation with a period of 180° (i.e. two-fold periodicity) which we argue is due to residual strain within the crystal, rather than being intrinsic. In addition, within the magnetically ordered zigzag phase there is a 60° period (i.e. six-fold) sawtooth pattern, which can be explained by reorientation of the zigzag domains as the crystal rotates in the applied field. Suppressing the zigzag order with an applied field above ~ 8 T at low temperature, a six-fold *sinusoidal* signal remains, suggesting that there is fluctuating zigzag order in the putative field-induced quantum spin liquid state. Finally, our key finding is a sharp, step-like feature that appears at low temperature for fields just above the zigzag phase boundary, at the so-called B2-axes. This is similar to theoretically predicted behaviour for a state with Ising topological order, which is expected for a Kitaev spin liquid in an applied magnetic field.

I. INTRODUCTION

Quantum spin liquids have generated interest both as a new phase of condensed matter and for their potential applications in the fields of quantum computing and spintronics, where they offer a paradigm-shifting alternative to traditional electronics. The recent incorporation of spin-orbit coupling has played a key role [1–4], by making *topological* quantum spin liquids theoretically possible. The analytically solvable Kitaev model, with bond-dependent Ising-type interactions of $J_{\text{eff}} = 1/2$ nearest-neighbours on a 2D honeycomb lattice, leads to frustrated spins and an emergent topological quantum spin liquid (QSL) [5]. With no applied magnetic field this QSL is found to host emergent excitations of gapless Majorana fermions and gapped Z_2 vortices - novel excitations should they be found in nature. The possibility of realizing the Kitaev model in real materials has aroused considerable interest (for reviews see [6–10]), and of the various candidate materials α -RuCl₃, which is the focus of this paper, has been the subject of several experimental and theoretical studies.

The Kitaev Spin Liquid ground state has limited stability in the presence of competing exchange interactions, and at zero field α -RuCl₃ displays zigzag antiferromagnetic order below $T_N \sim 7$ K (Fig. 1c). The current understanding is that a minimal description must include a ferromagnetic nearest-neighbour Kitaev interaction, Heisenberg interactions extending to at least the third neighbours, and an off-diagonal Γ term [11] that couples nearest-neighbour spins (see e.g. [12] for a discussion, and [13] for x-ray scattering results determining the interaction strengths).

Above a modest field of ~ 7.5 T applied in the ab -plane, neutron diffraction shows that zigzag order is sup-

pressed [16], and intense interest has focused on the magnetic field range $7.5 \text{ T} \lesssim B \lesssim 11 \text{ T}$, which we refer to as the “intermediate field phase”. This interest is enhanced by measurements that are consistent with predictions that a Kitaev spin liquid in an applied field will be a chiral spin liquid, with a gap that closes for fields parallel to certain high symmetry directions [17–19]. In particular, thermal Hall measurements showed a half-integer quantized thermal Hall effect [20], which is an expected signature of this phase. Moreover, angle- and field-resolved specific heat measurements, in the intermediate field phase [19], were interpreted in terms of gapped quasiparticle excitations, with a gap that closes when the applied field is parallel to the Ru-Ru bonds, as predicted by theory [5]. (Fig. 1a shows a schematic of the bond directions.) Other evidence for Kitaev physics includes temperature dependence of specific heat measurements [16, 21–23] showing a predicted double-peak structure in $C(T)$, although only the upper peak, near 100 K, has the predicted release of $0.5 R \ln 2$ expected for Majorana fermions.

The quantized thermal Hall effect measurements have been difficult to reproduce outside a few labs [24, 25], and alternative explanations have been suggested for the origin of the result, including phonons [26] and topological magnons [27]. Thus there is a clear need for other measurements that could show signatures of a field-induced topological spin liquid.

Our particular motivation for measuring the torque was a prediction by some of us [17], summarized in §IV:E, that the angle-resolved torque response of a state with Kitaev Ising topological order, of the kind consistent with the fractional thermal Hall measurements, should have a negative slope at the B1-axis (defined in Fig. 1a), with the slope becoming more negative as $T \rightarrow 0$ K. This prediction is made for a generic spin model [11].

In this study we report on the magnetization of α -RuCl₃ through measurements of the angle-resolved

* stephen.julian@utoronto.ca

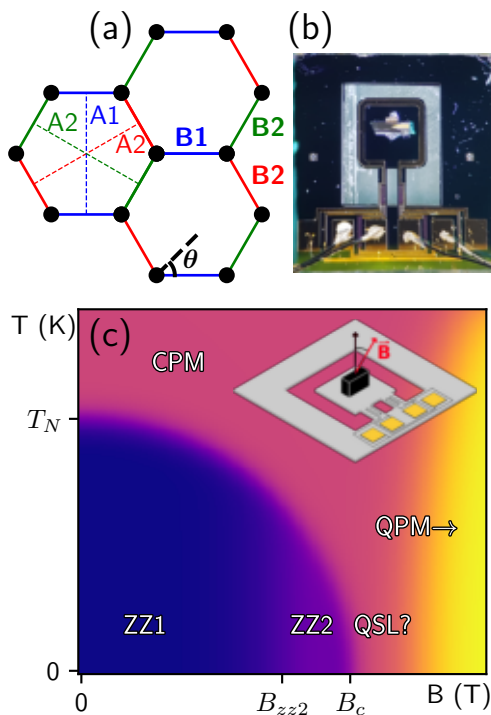


FIG. 1: (a) The three X,Y,Z Ru-Ru bond directions of α -RuCl₃: the *b*-axes are B1 (the C_2 axis for a crystal with monoclinic symmetry), and two equivalent B2 axes. For $R\bar{3}$ symmetry, B1 and B2 are equivalent. The complementary *a*-axes, A1 and A2, are shown as dashed lines. The nomenclature is borrowed from Lampen-Kelley et al. [14]. (b) Top view of sample L7K mounted on the Quantum Design torque chip P109A. (c) Cartoon phase diagram of α -RuCl₃. Above the zigzag ordering temperature $T_N \simeq 7$ K, α -RuCl₃ is in the classical paramagnetic phase (CPM). At zero field, below T_N α -RuCl₃ has zigzag antiferromagnetic order (ZZ1). Increasing the field beyond a threshold B_{zz2} induces a new zigzag ordering (ZZ2) [15]. Zigzag order is suppressed for fields beyond $B_c \sim 7.5$ T, at high field reaching a field-induced quantum paramagnetic state (QPM). In the intermediate field phase that lies between the ZZ2 and the QPM phases, we have found a step-like discontinuity and features that have been proposed for the Kitaev spin liquid (see IV). Inset: Cartoon depicting the angle-resolved torque magnetometry setup. The arrows represent the field direction, and the vector for the magnetic moment of α -RuCl₃.

torque, τ , in applied in-plane fields of up to 9 T in the temperature range of 2 - 20 K. We have measured several single crystals and find that the torque behaviour is sample dependent. In this paper we present results for a large, high-quality, $T_N = 7$ K crystal. Below, and in the Appendices, we justify this choice, presenting results on the sample dependence of the torque, and the effects of thermal cycling.

Our study complements previous torque studies of α -

RuCl₃, some of which focused on the torque or the related magnetotropic coefficient for out-of-plane applied fields ([28–30]), while the only previous torque study for in-plane fields that we are aware of seems, in light of our results, to have been affected by strong residual C_2 strains [31].

Our results are more complex than predicted for a pure Kitaev interaction: just outside the boundary of the zigzag phase we see a sinusoidal six-fold-symmetric signal, but rather than reflecting a closed gap on the honeycomb bond direction, it may be indicative of short-range fluctuating zigzag order. At low temperature, however, a sharp signature with negative slope is observed at the B2-axes (defined in Fig. 1a) as soon as the intermediate phase is entered from the zigzag phase. This signature is similar to the theoretical prediction [17].

We also report, within the zigzag phase, the existence of strong sawtooth steps with six-fold symmetry, and at all fields at all temperatures, a two-fold torque signal that is sample and also sample-history dependent, which leads us to conclude that it is probably not intrinsic.

II. EXPERIMENT

We measured single crystals of α -RuCl₃ that were grown using chemical vapor transport as described in previous work [26]. Two grams of α -RuCl₃ powder (Sigma-Aldrich, Ru 45-55%) were sealed in a quartz tube under vacuum. The quartz tube was heated in a two zone furnace where the temperature gradient was kept at 70 °C. The powder was initially heated at 850 °C for two days, followed by cooling at 4 °C/h down to 600 °C.

In all we checked the torque response of 14 single crystals, thirteen of which were “small”, measuring $\sim 100 \times 50 \times 50 \mu\text{m}^3$, suitable for measurement with miniature piezoresistive cantilevers (Seiko Instruments PRC120). The most extensive set of measurements was done on a “large” single crystal, measuring $\sim 1 \times 0.6 \times 0.3 \text{ mm}^3$, with a 7 K transition (sample L7K), placed on a Quantum Design Torque Chip P109A (Fig. 1b). For reasons presented below, and in the Appendices, we believe this to be the highest quality sample, and it is thus the focus of this paper. The crystal was held in position on the PPMS chip by an L-bracket of copper sheet and a light layer of vacuum grease (as shown in Fig. 1b), with the c^* -axis aligned parallel to the axis of rotation and perpendicular to the magnetic field. This sample (L7K) has additionally been characterized with x-ray diffraction to confirm its orientation. Measurements at low field strengths (2 T) confirmed a T_N of ~ 7 K, in line with previous literature suggesting a sample with correct ABC stacking.

All measurements were done using a Quantum Design PPMS, using the Horizontal Rotator option, at temperatures between 2 and 20 K, and fields from 0 to 9 T. In the majority of our measurements the crystal was rotated such that the applied field swept through 180° or 360° in

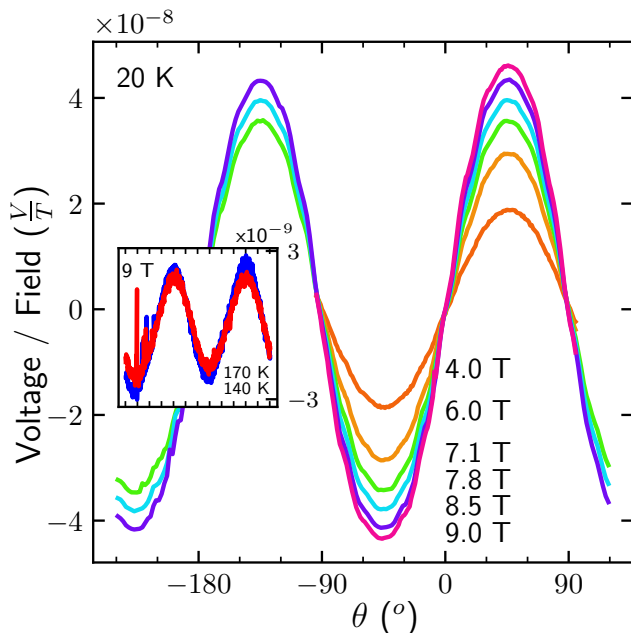


FIG. 2: At 20 K the torque is dominated by a clear 180° (i.e. two-fold) signal that grows strongly with field. At all fields this acts as a significant background to the more interesting higher-frequency signals. Inset: 9 T measurements at 140 K and 170 K, showing that the two-fold signal persists up to and beyond the structural transition.

the ab -plane, while the temperature and the magnitude of the field were held constant. In all of the 360° studies the torque consisted very precisely of two repeated 180° patterns, as expected. In a few cases we swept temperature or field at fixed angle, to check T_N or to look for quantum oscillations.

In all of our plots, angles have been translated so that 0° and -180° are at the B1 axis. Moreover, torque is given in volts (or volts per tesla) which was the signal from a Wheatstone bridge that measured the twisting of the sample platform. A calibration measurement, outlined in the Appendix (§C), provides a conversion factor of $(17 \pm 4) \times 10^{10} \text{ Nm}^{-2}/\text{V}$ between these voltages and the torque density in Nm^{-2} .

III. RESULTS

Our torque signals can be decomposed into oscillations with distinct periods as a function of angle, and in this section we discuss them in sequence starting with two-fold (180° period) signals, before turning to six-fold signals which are a focus of later discussion. We finally discuss sharp steps, or peaks, observed in the intermediate field phase at low temperature near the B2-axes.

180° Periodic Signal: A clear 180° periodic signal appears in all of our torque vs. angle measurements. Fig. 2

shows a baseline series of measurements at 20 K at fields between 4 and 9 T on sample L7K, in which a 180° signal, that scales with field as H^2 , dominates the torque. Assuming that the sample is crystallographically single-domain, this 180° background signal reflects C2/m symmetry of the individual layers of $\alpha\text{-RuCl}_3$, with a primary a -axis (A1) that is perpendicular to the Ru-Ru honeycomb bonds, and b -axis (B1) parallel to a Ru-Ru bond (see Fig. 1a). The angle-resolved torque vanishes at both of these axes. In all of our plots we have shifted the origin of the horizontal axis so that B1 is at 0° and -180° , while A1 is at $\pm 90^\circ$. As shown in the inset of Fig. 2, the 180° periodic contribution persists up to, and beyond, the structural transition $T_c \sim 140 - 160\text{K}$ [32].

The 180° periodic signal is moderately enhanced as $T \rightarrow 0\text{K}$. This can be seen in Fig. 3a, which shows the angle-dependent torque at 4 T at various temperatures. Additionally, with decreasing temperature a pronounced six-fold (60°) contribution appears. Fig. 3b shows the temperature dependence of the Fourier amplitudes corresponding to the 180° and 60° components. It is evident that these components are independent. From this, and further analysis in the Appendix, we justify the choice to subtract off the 180° sinusoidal component in our future analyses and plots.

60° Periodic Signal: We turn now to the 60° periodic signals. These signals are very prominent in our sample within the zigzag ordered phase, but only for sufficiently strong fields. For example, as seen in Fig. 4, at 2 K (i.e. deep within the zigzag ordered phase) the torque at 0.5 T, after a subtraction of the two-fold contribution, is nearly constant with no notable features, while a field of 1.2 T induces a weak 90° periodic contribution. At 4 T, however, the six-fold sawtooth pattern emerges very clearly. In Fig. 3b it can be seen that the Fourier amplitude of the 60° periodic component is negligible for $T > T_N$, but grows rapidly upon entering the zigzag phase. Fig. 4 shows that increasing the strength of the applied field beyond 4 T within the zigzag phase distorts the signal from a clean sawtooth, with the step-like features increasing in amplitude across the A1-axis, while decreasing across the A2-axes. We discuss the implication of this distortion with respect to a coupling of the 180° and 60° periodic contribution to the signal in §IV:C. The sawtooth signal is fully suppressed at $\sim 8\text{T}$, as the intermediate field phase is entered. This same trend can be seen at other temperatures $T < T_N$ in Fig. 5(a-d), where the signatures of a sawtooth signal can be seen up to 7.8 T at temperatures as high as 6 K.

We argue in §IV:A that this sawtooth signal arises from rotation of zigzag domains as the sample rotates in the applied field, and that it is thus an indicator of good sample quality. There we show that the steps of the sawtooth signal are expected to align with the a -axes (i.e. A1 and A2 of Fig. 1a). We note that the orientation determined this way is consistent with x-ray diffraction at room temperature, but the structural transition at $\sim 140 - 160\text{K}$ means that additional information is needed in order

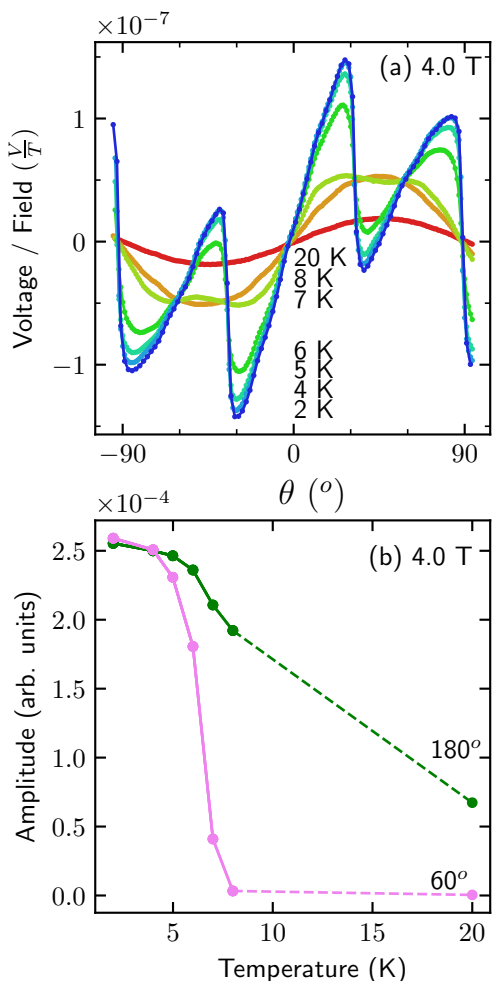


FIG. 3: (a) Angle-resolved torque measurements at 4 T for $2 \text{ K} < T < 20 \text{ K}$. A nearly pure 180° periodic signal for $T \gg T_N$ is distorted starting at $\sim T_N$, gaining a 60° periodic signal which quickly transforms into a sawtooth pattern. (b) Fourier amplitudes of the 180° (green) and 60° (pink) periodic contributions to the signal in (a), plotted against temperature. The 60° periodic contribution activates abruptly at $T \sim T_N$.

to orient the crystals at low temperature. Locating the a -axes at the steps in the sawtooth, together with the alignment of the zero-crossings of the torque with the B1- and A1-axes at 20 K, determines the orientation of our crystal at low temperature.

A novel finding of this study, presented in Fig. 5, is that a sinusoidal 60° torque signal persists outside of the zigzag phase, within the putative intermediate field Kitaev state. At 4 T a six-fold sinusoidal signal can be seen in a narrow temperature range below 7 K, within the zigzag phase, as in Fig. 5a. At higher fields, but still with $B < B_c$, the temperature range expands: the sinusoidal signal now appears at higher temperatures *outside* the zigzag phase, as well as at lower temperatures within the zigzag phase, before giving way to the sawtooth signal

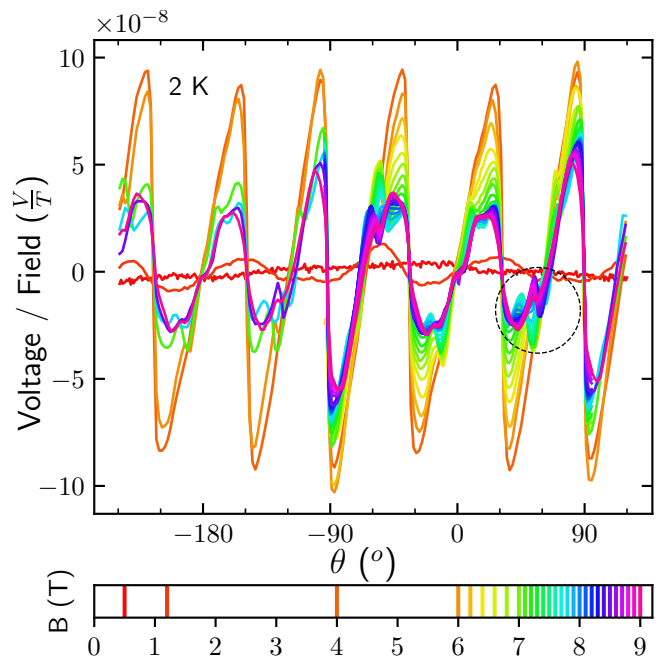


FIG. 4: Angle-resolved torque of L7K at 2 K. A temperature-dependent 180° periodic sine wave contribution has been subtracted. At low field the torque response is constant, as expected. A 90° periodic contribution is present at 1.2 T, and the signal further develops into a 60° periodic sawtooth signal by 4 T. The sawtooth discontinuities are present at each equivalent a -axis (ie. $\pm 30^\circ, \pm 90^\circ, \dots$). The sawtooth signal distorts as field strength is increased, with intermediate features developing between each discontinuity, and with the overall signal amplitude decreasing. Inflection points form along the b -axes (ie. $0^\circ, \pm 60^\circ, \dots$) with increasing field, which invert across the B2-axes ($\pm 60^\circ, \pm 120^\circ$) upon exiting the zigzag phase. The circled region is discussed below as a possible signature of Kitaev physics (see §IV-D).

at still lower temperatures. Above B_c , again *outside* of the zigzag phase, the 60° sinusoidal signal persists down to the lowest temperatures measured.

Features of multiple zigzag phases: The transition from zigzag order to the intermediate field phase is complicated by an intervening zigzag phase, denoted as zigzag 2, as opposed to zigzag 1 at low field, (see Fig. 1) with a critical field that varies strongly with field angle [33, 34]. In the region between about 6 and 7.7 T [33] where these transitions take place, we see in Fig. 5b-d sharp peaks whose position is field dependent. A plot of the position of these extrema vs. field and angle, however, reveals a pattern with little similarity to the accepted phase boundaries [33]. If the origin of these peaks is in the complex zigzag phase boundaries shifting with changing in-plane field angle, it is notable that both the large and small $T_N = 7 \text{ K}$ sample host these complex features, though the domain rotation is seen only in sample L7K (see Fig. 11 in the Appendix).

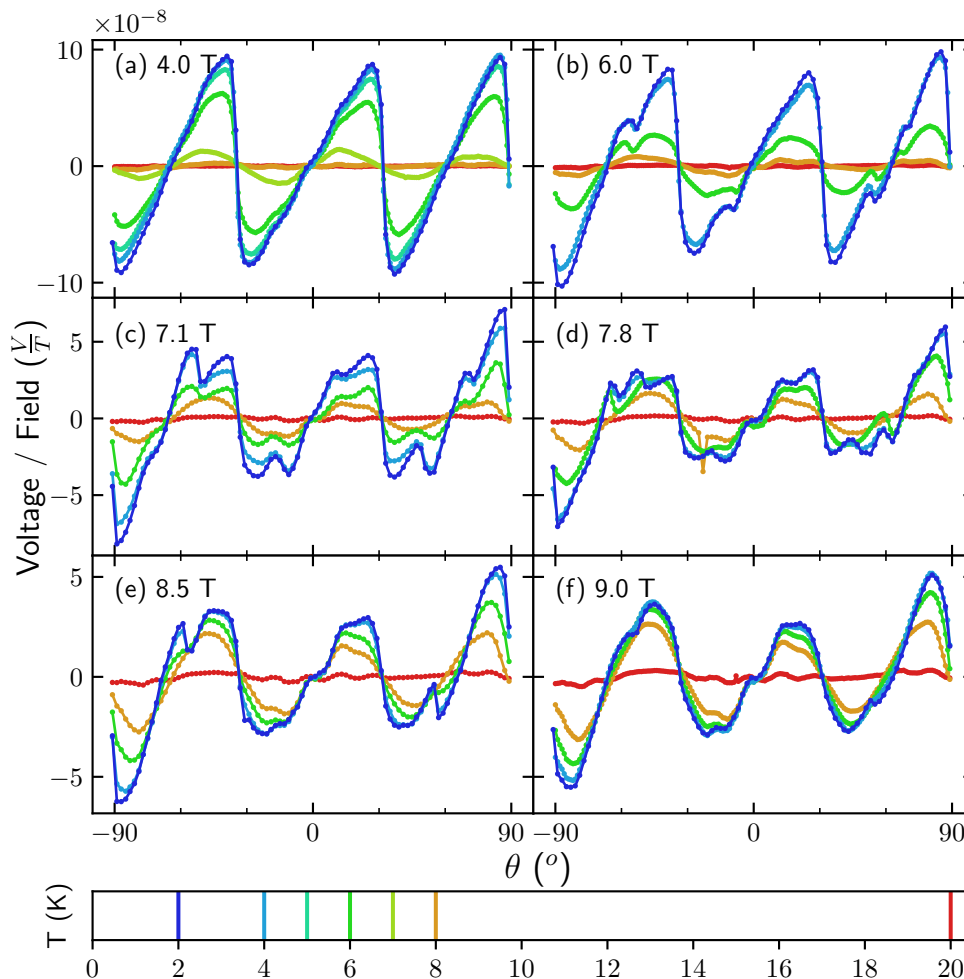


FIG. 5: Torque vs. angle in sample L7K at fixed fields, vs. temperature. A 180° sinusoidal contribution has been subtracted. (a) 4 T. At 8 K and above no features are present; 7 K shows a 60° sinusoidal contribution, without harmonic distortion. Below 7 K the sawtooth pattern grows rapidly. (b-d) 6, 7.1 and 7.8 T. The sawtooth steps weaken with increasing field, as a sinusoidal pattern emerges at higher temperatures. A complex pattern of intermediate local extrema appears. The sharp step at the A1-axes ($\pm 90^\circ$) may be due to harmonic distortion of the two-fold contribution. At the B1-axis (0°) a plateau appears and grows with increasing field. (e-f) The step at the A1-axes, and plateau at the B1 axis, persist. Several of the local extrema have decayed or disappeared, but a sharp peak, or step-like discontinuity, emerges near B2 ($\sim \pm 60^\circ$) at 8.5 T.

Features near symmetry axes: In Fig. 5d, e and f we see features in the immediate neighbourhood of the A1, B1, and especially, the B2 axes. At A1 there appears to still be a downward step, but we argue below that this is due to a combination of non-linear distortion of the magnetization and torque, and subtraction of a pure 180° sinusoidal contribution (see Fig. 8). In Fig. 6a we focus on the temperature evolution of B1 and B2 features at 8.5 T. At the zero-crossing marking the B1-axis (0°) the signal shows a plateau for temperatures below 8 K. The insets of Fig. 6a show the signal at B1 with both a 180° and a 60° periodic sine wave subtracted, showing that a negative slope in the residual signal across the B1-axis is enhanced with decreasing temperature (top inset), but that it is not field dependent for $B > 6$ T (bottom inset), so it is not a particular feature of the intermediate field phase.

In contrast, across the B2-axes a step-like discontinuity forms in the torque response that is only seen in the intermediate field phase at the lowest temperatures. At the B2 axes at 8.5 T, for example, there is an asymmetric, downward peak at $\sim 60^\circ$ whose left-hand side appears to be a discontinuous step, but that shows up only at 4 and 2 K (Figs. 5e, 6a), while Figs. 6b and 5c-e show that, at 2 K, the feature grows rapidly as the field is increased beyond 7.5 T. A comparison of this feature to the theory for a Kitaev spin liquid at high field is made in §IV-D.

IV. DISCUSSION

First we discuss the origin of the sawtooth pattern seen within the zigzag-ordered phase. We follow this with a brief discussion of the origin of the 180° periodic signal.

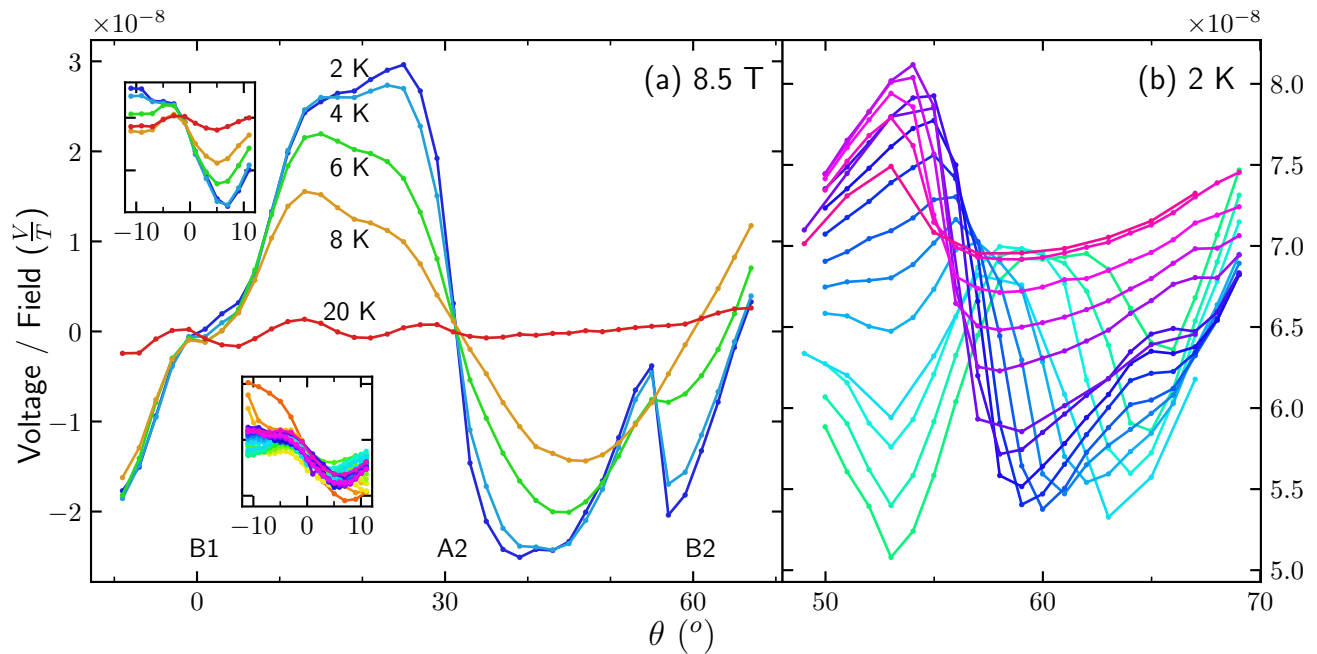


FIG. 6: (a) Zoomed-in window capturing the B1, A2, and B2 axes of sample L7K at 8.5 T. A 180° periodic sine wave has been subtracted. A plateau is seen across the B1-axis, and is only weakly temperature dependent. A steep step-like feature develops across the A2-axis (just as across the A1-axis) with decreasing temperature. Near B2, below a threshold temperature ~ 4 K, a sharp step-like feature develops. Top inset: Angle-resolved torque about the B1 axis at 8.5 T and temperatures from 20 K (red) to 2 K (blue), from which a further 60° periodic sine wave has been subtracted. Bottom inset: Angle-resolved torque about the B1 axis at 2 K and fields from 4 T (orange) to 9 T (purple), from which the additional 60° periodic sine wave has been subtracted. (b) The raw (no background subtraction) data of the angle-resolved torque near the B2-axis at 2 K, for magnetic fields from 7.5 T (green) to 9.0 T (purple) at evenly spaced intervals of 100 mT. The downward-step-like feature develops quite suddenly upon entry into the intermediate field phase, and is seen to move as the field changes.

We then discuss the non-sawtooth 60° periodic sinusoidal signal which develops in proximity to the antiferromagnetic region and persists into the intermediate field phase. Finally, the fine structure seen at the lowest temperatures with increasing field are discussed, focusing on the features that develop near the B1 and, especially, the B2 axes, and their possible connection to theoretical predictions for a Kitaev spin liquid.

A. Interpretation of the saw-tooth pattern

Crystal L7K shows a strong, six-fold, saw-tooth pattern in the zigzag ordered phase. This can be explained by the rotation of the zigzag domains to minimize their Zeeman energy, as is commonly observed in antiferromagnetic materials with C_3 or higher symmetry.

We can illustrate this behaviour with a simplified free energy of the form

$$\mathcal{F}_i = KL_i^2 - \vec{M} \cdot \vec{B}, \quad (1)$$

where $i = 1, 2, 3$ labels the domain, and $L_i = (M_{\perp,i}^A - M_{\perp,i}^B)$ is the zigzag order parameter, where $M_{\perp,i}^{A,B}$ is the

component of the magnetization on sublattice A/B that is perpendicular to Ru-Ru bond direction b_i .

The spin configurations at zero field and in a rotating applied field are illustrated in Fig. 7a,b. At zero field there are three equivalent zigzag domains (Fig. 7a). In an applied field, the L_i that minimizes the free energy is the one whose sublattice magnetizations are the ‘most perpendicular’ to the applied field \vec{B} , because this allows the spins on both sublattices to have a component parallel to \vec{B} while still optimizing their exchange energy (which favours antiparallel alignment of the sublattices).

The free energy of the three domains, from Eq. 1, and the resulting torque, $\partial\mathcal{F}/\partial\theta$, are shown in Fig. 7c. When the field passes through an a -axis, the minimum free energy switches from one zigzag domain to the next. When this happens, the magnetization vector switches from one side of \vec{B} to the other, causing a step in the torque. We note that a calculation of the magnetization from this simplified model closely mimics M/B vs. angle measurements at 3 and 5 T shown in Fig. 3g of Ref. [33]. Thus, our sawtooth pattern and its explanation in terms of rotating zigzag domains are consistent with earlier magnetization measurements, and with more sophisticated theoretical modeling (e.g. [12]). It differs however from

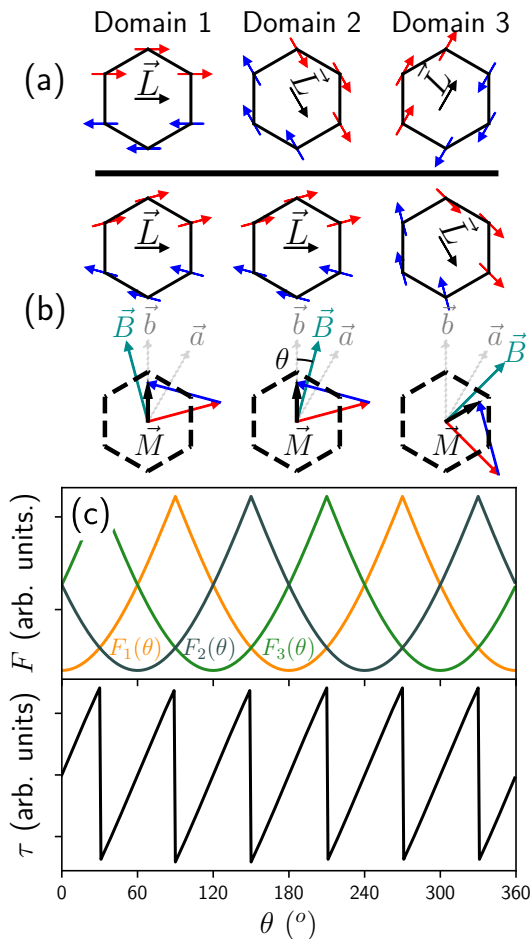


FIG. 7: (a) The three equivalent zigzag spin domains at zero field. The exchange energy in our simplified model depends only on the component of the magnetization that is perpendicular to a Ru-Ru bond (i.e. to a b -axis). (b) In the presence of an applied field, L_i switches to keep $\vec{M}_{\perp,i}$ as perpendicular to the applied field as possible, minimizing the exchange-plus-Zeeman energy. The net magnetization, \vec{M} , is given by the sum of the two sublattice magnetizations. As \vec{B} passes through an a -axis the magnetization \vec{M} switches from one side of \vec{B} to the other, causing a step in the torque. (c) Top: Free energy of the three domains as a function of field angle. Bottom: The calculated torque, which jumps as the free energy minimum switches between domains.

a recent interpretation of magneto-optical spectroscopy which argued that for $B \parallel \vec{a}$ the zigzag order ultimately rotates such that the spins are perpendicular to that a -axis [35]. This would not produce steps in the torque.

A sample in which the domains were pinned and unable to rotate would not produce a six-fold signal in the zigzag phase even if all three domains were equally stable at zero field; nor would a six-fold signal appear in a sample with single-domain zigzag order due, for example, to strong residual C_2 strain. As shown in the Appendix,

our much smaller samples, having T_N of both 7 K (S7K) and 14 K (S14K), do not show six-fold sawtooth torque in the zigzag ordered phase, which would be consistent with either of these scenarios, though which is correct is unclear.

B. Two-Fold Contribution

All of the samples we measured exhibit a strong 180° periodic signal. The results for sample LK7 are shown in §III (see Fig. 2), while results for our small samples are shown in the Appendix. Previous studies have assumed that 180° periodicity, reflecting C_2/m symmetry of the crystal, involves a shortened Ru-Ru bond along a primary b -axis [36], which in our notation would be the B1 bond.

The measurements presented in the Appendix suggest that this 180° periodic contribution is not intrinsic to α - RuCl_3 at low temperature, but is instead a result of residual strain in the sample, perhaps either from cooling through the ~ 150 K structural transition too quickly, or from the way the crystals are mounted, with one end stuck to the cantilever with grease. This offers a natural explanation of why, for example, thermal cycling enhances the 180° periodic contributions, without affecting the six-fold signal (see Fig. 10, in the Appendix), and why the torque in our small crystals is dominated by the 180° signal. Moreover, other measurements by some of us [37] support the notion that the low-temperature structure is $R\bar{3}$.

It seems that most studies on samples with predominantly $R\bar{3}$ symmetry still show varying degrees of residual C_2 symmetry at low temperature, and it may be that samples have to be cooled very slowly, in strain-free conditions, to show pure $R\bar{3}$ symmetry (e.g. [21, 33, 38]).

We note that, despite the C_2 symmetry signal observed in sample LK7, evidently this strain is not sufficient to prevent the rotation of magnetic domains in the zigzag state.

C. Six-fold signal in the intermediate field phase

The sinusoidal 60° periodic signal appears to be a distinct but related phenomenon from the sawtooth signal seen in the zigzag phase. Both at the boundary to the zigzag phase at low fields, and at low-temperatures in the intermediate field phase, this sinusoidal signal persists where the sawtooth signal is absent. The presence of the sinusoidal six-fold signal at 4 T, just below the boundary to the zigzag phase, perhaps offers some insight to what the signal represents. We know that in this region static zigzag order has set in, and the existence of a six-fold signal tells us that the zigzag order has a preferred domain, but the sinusoidal nature of the signal tells us that fluctuations are still large enough that all of the domains are partially populated, with populations that vary smoothly as the direction of the field changes.

Fig. 10b (in Appendix A) shows that, at 9 T, the six-fold sinusoidal signal in the intermediate field phase grows gradually below 20 K, before saturating below ~ 4 K. Given the same form of the signal just below T_N at 4 T, and at 9 T below 20 K, the most logical interpretation is that the six-fold signal outside the zigzag phase is due to fluctuating zigzag order.

A simplified model the fluctuating order can be made using a free energy with anisotropic six-fold susceptibility as well as C_2 symmetry breaking, of the following form:

$$\mathcal{F}(\mathcal{M}, \theta, \phi) \simeq \frac{1}{2}(\chi_0 + \chi_2 \cos(2\phi) + \chi_6 \cos(6\phi))^{-1} M^2 - MB \cos(\theta - \phi), \quad (2)$$

where M is the magnetization, θ is the angle of the applied field within the plane, and ϕ is the angle that the magnetization vector \vec{M} makes within the plane. As usual, angles are measured from the B1 axis.

For a given field \vec{B} , \mathcal{F} is minimized with respect to M and ϕ , and the torque calculated from $\tau_z = M_x B_y - M_y B_x$.

In Fig. 8 we show sample results, where \mathcal{F} has been minimized numerically. An important point is that the anomalous behaviour at the A1 axis, which is apparent after a 180° background has been subtracted (see Fig. 8b) is explained by non-linear coupling between the χ_2 and the χ_6 terms, which produces harmonic distortion. If instead of Eq. 2 we use a linear prefactor for M^2 (i.e. of the form $(\chi_0^{-1} + \chi_2^{-1} \cos(2\phi) + \chi_6^{-1} \cos(6\phi))$), then this anomaly at A1 is not reproduced. Thus, the enhanced peaks near the A1 axis, seen, for example in Fig. 5e and f, are not a special feature of the six-fold physics. This interpretation suggests, incidentally, that the two-fold and six-fold signals originate in the same regions of the crystal.

Short-range zigzag order outside of the zigzag phase is not surprising. After all, inelastic neutron scattering measurements see a strong six-fold anisotropy in the magnetic scattering well above T_N [39], while specific heat measurements (e.g. [23]) clearly show an upturn as T approaches T_N from above, which is a signature of fluctuating short-range order. Nevertheless, we do not have an explanation for why such fluctuating order should be stronger at high field than at low field, that is, why we do not see six-fold sinusoidal signal at 4 T for $T > T_N$, but we do see it at 6 T and above. Regarding the intermediate field phase in the limit as $T \rightarrow 0$ K, in the Introduction we mentioned specific heat measurements [19] that found an apparent gap-closing six-fold anisotropy with an excitation gap that closes for $\vec{B} \parallel \vec{b}$. This was interpreted in terms of field-induced Kitaev Ising topological order, but our results suggest that fluctuating zigzag order should also be taken into consideration. A possible interpretation is that, because zigzag order is suppressed at 7.2 T for $\vec{B} \parallel \vec{a}$, as opposed to 7.7 T for $\vec{B} \parallel \vec{b}$ [33], then at 8 T, where specific heat measurements [19] see the strongest six-fold anisotropy, fluctuating zigzag order

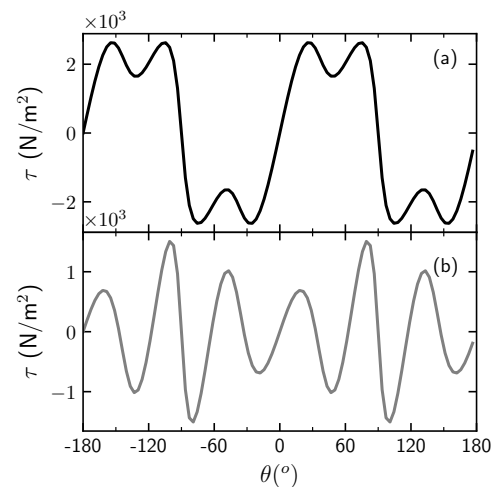


FIG. 8: (a) Torque density vs. angle for the free energy of Eq. 2. (b) After subtracting the two-fold contribution there is a downward step-like feature at $\pm 90^\circ$, as observed in the data at low temperature and high field (see Fig. 5e and f, and 11b).

is largest along the b -axis simply because we are closer to the quantum critical point for suppression of zigzag order.

D. Comparison of torque signals in the intermediate phase with the theory for Kitaev Ising topological order

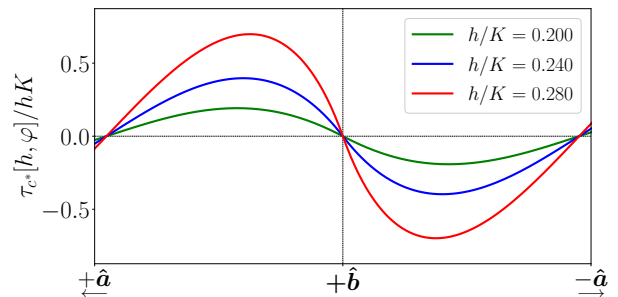


FIG. 9: Torque vs. angle calculated by Gordon and Kee [17].

Theoretical Predictions: Kitaev [5] finds that, in an applied magnetic field, the itinerant Majorana fermions (MF's) of the Kitaev spin liquid become gapped, and they acquire a nontrivial Chern number. The resulting phase has Ising topological order (ITO).

The ITO is prohibited when the external field is parallel to a b -axis since the pseudo-mirror symmetry is unbroken. As the field sweeps across such a C_2 axis the Chern number switches from $+1$ to -1 , and at the axis itself the gap must close. Gordon and Kee [17] noted that this topological transition leads to a sharp cusp singularity in

the magnetotropic coefficient, which is independent of the details of microscopic spin interactions, as this special C_2 symmetry is a property of the generic spin model. Writing the energy of the MF's as $\varepsilon_{\pm} = \pm\sqrt{(vq)^2 + m(\varphi)^2}$, where $m(\varphi)$ is the mass and v is the velocity of the MF's, the free energy at $T = 0$ is given by the integral over q of the lower branch:

$$\begin{aligned}\mathcal{F} &\simeq \frac{1}{2} \frac{A}{(2\pi)^2} \int_{vq < \Lambda} d\vec{q} \varepsilon_{-}(\vec{q}) \\ &= \frac{A}{12\pi v^2} \left[|m|^3 - (\Lambda^2 + m^2)^{3/2} \right],\end{aligned}\quad (3)$$

where $\Lambda \gg m$ is an ultraviolet cutoff and A is the area of the honeycomb unit cell. Gordon and Kee [17] focus on the singular $|m|^3$ part of \mathcal{F} , which yields a cusp in the magnetotropic coefficient, $\partial\tau/\partial\varphi$. This singular part may, however, be only weakly observable in the torque τ , which we obtain from:

$$\begin{aligned}\tau &= \frac{\partial\mathcal{F}}{\partial\varphi} = \frac{A}{2\pi v^2} \left[3m^2 - \frac{3}{2}(\Lambda^2 + m^2)^{1/2}m \right] \frac{\partial m}{\partial\varphi} \\ &\simeq -\frac{3A}{4\pi v^2} \Lambda m \frac{\partial m}{\partial\varphi}.\end{aligned}\quad (4)$$

The mass (i.e. the gap) is proportional to the angle between the applied field, φ , and the C_2 axis, φ_* : $m \propto \delta\varphi = \varphi - \varphi_*$. Thus, according to this calculation the torque at the C_2 axis passes through zero (as required by symmetry) but with a *negative* slope. The physics is relatively simple: the energy is lowered if the sample rotates the C_2 axis away from the field, because this increases the gap $m(\varphi)$, lowering the entire MF spectrum $\varepsilon_{-}(\vec{q})$. This expected behaviour is shown in Fig. 9.

Tanaka et al. [19] present strong evidence from specific heat for the closing of a gap at all of the b -axes in α - RuCl_3 , which would be consistent with Ising topological order for $R\bar{3}$ symmetry. The closing of the gap is visible below about 5 to 10 K, but becomes increasingly clear as $T \rightarrow 0$ K. Thus, in torque in the intermediate field phase, if our sample has the same crystallographic symmetry as that used by Tanaka et al., and Ising topological order is the relevant physics as opposed to, say, proximity to the zigzag quantum critical point, we should expect that the torque acquires an increasingly negative slope at the b -axes as the temperature is decreased below 10 K. If, on the other hand, our sample has C_2 symmetry rather than $R\bar{3}$ symmetry, then the negative slope would occur only at the B1 axis. We instead see a negative slope with strong temperature dependence around the two B2-axis crossings, not across the B1-axis.

Experimental Results: Within the zigzag-ordered phase we know that the slope of the torque is positive at the b -axes: from our model, the magnetization rotates *toward* the applied field in the zigzag phase. On the other hand, with the nearly pure 180° signal seen at 20 K (Fig. 2), the slope is positive at the B1 axis but weakly negative at B2.

To look for a negative slope in the intermediate field region at the B1 axis, we first subtracted the strong 180°

signal, giving the results shown in Figs. 5 and 6. Even after this subtraction, however, we are left with the residual sinusoidal 60° signal discussed above, which has a positive slope at the B1 and B2 axes. In light of this we have also subtracted the six-fold sinusoidal (upper inset in Fig. 6a). After this subtraction the plateaus of Fig. 6 indeed yield a negative slope at the B1 axis, but the temperature dependence is rather weak and the field dependence is even weaker: the residual negative slope persists deep into the zigzag phase (bottom inset of Fig. 6), so the B1 axis torque does not appear to conform to the prediction for Ising topological order.

The B2 axis is not trivial to locate. We expect it to be at $\pm 60^\circ$, but perhaps due to interaction with the C_2 magnetization, we believe from the symmetry of the signal that the magnetic B2 axis is shifted to slightly lower angles compared to the crystallographic B2 axis. The approximate location of the isosbestic points (see Fig. 6a and b) suggests that the magnetic B2 axis, in the intermediate field phase, is located between 56° and 58° .

At that angle, within the zigzag phase (i.e. below 7.5 T) the slope is positive, but it rapidly becomes large and negative as the field increases to 8.5 T, before becoming smaller up to 9 T. Fig. 6 shows that at 8.5 T this feature corresponds to a sharp downward step that produces what appears to be a discontinuity in the torque across the B2 axis. Although this step is not smooth like the predicted torque pictured in Fig. 9, this may be due to the limited angular resolution in our measurement. The step has the negative sign predicted in the theory and it increases rapidly in size with decreasing temperature (see Fig. 6a), also as predicted. Moreover, although this step may look similar to the many peaks and steps that we see in Fig. 5 between 6 and 7.8 K, we believe that it is different: all of these other features fade upon entry into the intermediate field range, while this one is strongest in the intermediate field phase, just above the zigzag phase boundary. In this it is also distinct from the negative slope of the (background-subtracted) signal at the B1 axis.

Finally, this step is not explainable with the model we used for the steps in the zigzag phase: zigzag order can produce only positive-slope features at the b -axes, nor is the step explainable by any other physics that we are aware of. Thus, while it does not exactly conform to the theoretical model, largely because it occurs at the B2 instead of the B1 axis, the curves for fields between 8 and 9 T in Fig. 6b bear a striking resemblance to the theoretical prediction illustrated in Fig. 9, making this the most promising feature we have found that could be a signature of the field-induced Kitaev state. It would be worthwhile to explore it with other probes, especially direct measurements of the magnetotropic coefficient [28, 29].

V. CONCLUSIONS

Comparing the torque vs. angle between three different samples, across a large region of the temperature-magnetic field phase space has led us to following conclusions.

1. Two-fold anisotropy of the magnetization is both sample dependent and sample-history dependent, and is probably not intrinsic to the true crystallographic ground state of α - RuCl_3 .
2. Within the zigzag ordered phase, high quality crystals show a strong six-fold sawtooth pattern in the torque, that is explained by rotation of the zigzag domains to minimize the magnetic interaction energy with the applied field.
3. In the high-field intermediate field phase, there is a sinusoidal six-fold contribution to the torque that is opposite in sign to the predictions for a field-induced Kitaev state, but that may be due to fluctuating zigzag order, a finding which may have implications for the interpretation of zeros in the gap at the b -axes found by specific heat measurements [19].
4. In the intermediate field phase, there are however sharp step-like features in the torque at the B2 axes that have many of the features predicted for field-induced Kitaev Ising topological order, and for which we have no alternative explanation. These features thus offer a promising route for future investigations.

ACKNOWLEDGMENTS

This research was supported by the Natural Sciences and Engineering Research Council of Canada (NSERC RGPIN-2019-06446). S. Kim and Y.J. Kim acknowledge the Natural Sciences and Engineering Research Council of Canada (RGPIN-2019-06449, RTI-2019-00809), Canada Foundation for Innovation, and Ontario Research Fund. J. Gordon and H.Y. Kee acknowledge support from the Natural Sciences and Engineering Research Council of Canada Discovery Grant No. 2022-04601. H.Y. Kee also acknowledges the Canadian Institute for Advanced Research, and the Canada Research Chairs Program.

Appendix A: Thermal Cycling Effects

Most of our measurements on sample L7K were conducted during a single (first) cooldown from room temperature, but followup measurements were carried out after thermally cycling the sample to room temperature

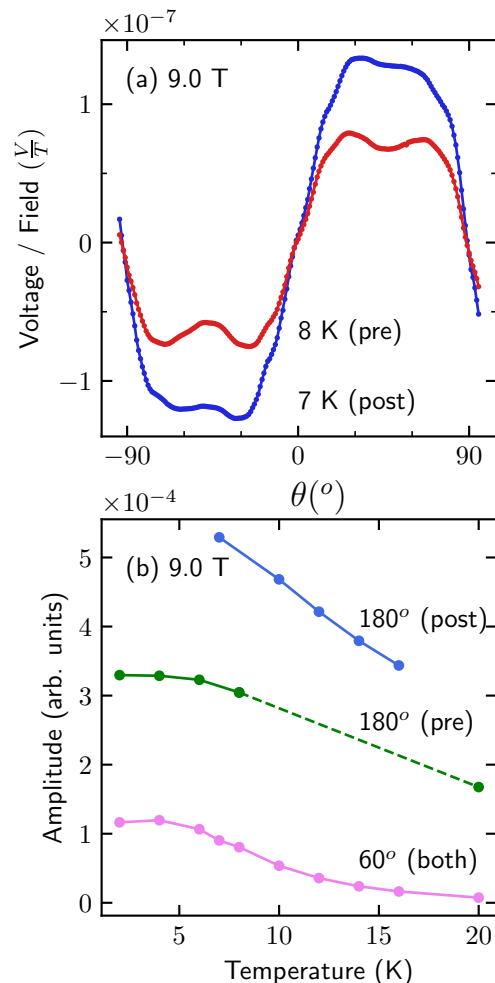


FIG. 10: (a) Angle-resolved torque response for sample L7K, before (pre) and after (post) thermally cycling the sample to room temperature. Thermal cycling enhanced the 180° periodic contribution to the signal, while minimally affecting higher-frequency contributions. (b) Sample L7K Fourier amplitudes vs. temperature at 9 T, including measurements from before and after thermally cycling the sample. The $C2/m$ contributions are enhanced by thermal cycling, while the $R\bar{3}$ contributions, labelled ‘ 60° ’, are relatively unchanged. In both figures, the connecting lines are guides to the eye.

and back to low temperature, and it was found that thermally cycling sample L7K enhanced the 180° periodic contribution to the signal. As shown in Fig. 10, at 7 K after thermal cycling the 180° contribution is approximately twice as large as at 8 K before cycling. Fig. 10b shows the amplitude of the 180° periodic contribution, extracted by Fourier analysis, as a function of temperature. It can be seen that the 180° periodic contribution is enhanced at all measured temperatures. In contrast, a 60° periodic contribution to the signal (pink line in Fig. 10) is unaffected by thermally cycling the sample.

Appendix B: Comparisons of Sample Quality

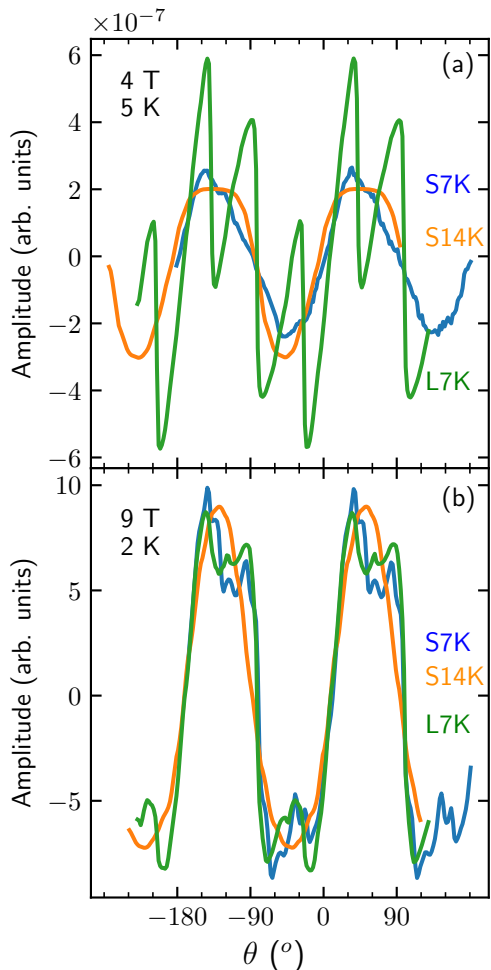


FIG. 11: Illustrating the differences between samples. (a) Torque vs. angle of samples S7K, S14K and L7K, at 4 T and 5 K. A multiplicative factor has been applied so that the amplitude of the 180° periodic contribution is the same across datasets. Only sample L7K shows a 60° periodic sawtooth, superposed on the 180° signal. (b) Angle-resolved torque response of samples S7K, S14K and L7K at 9 T and 2 K. Sample S14K shows only a 180° periodic contribution, while both samples S7K and L7K exhibit a complex series of higher-frequency contributions superposed on a strong 180° signal.

Over time, the understanding of sample quality has evolved [40] to capture the effects of stacking faults, and sample shape and size. A major distinction is between samples in which zigzag order sets in at 7 K vs. 14 K, which is now understood to reflect different stacking of the honeycomb planes [40]. The 7 K stacking has become the accepted ideal for experimental measurements [41], such crystals having what is believed to be the intrinsic

stacking (ABCABC), whereas $T_N = 14$ K samples have an (ABAB) stacking.

As discussed in Appendix A, the 180° periodic signal is probably not intrinsic to the low-temperature structure of α - RuCl_3 , but rather indicates residual strain within the sample. We note, moreover, that small crystals seem more disordered than our large crystal, regardless of T_N . Both a small $T_N = 7$ K sample (S7K) and a small $T_N = 14$ K sample (S14K) exhibit strong 180° periodic behaviour (see Fig. 11), but within the zigzag-ordered phase neither sample shows the clearly defined 60° periodic sawtooth signal of our large crystal L7K. A possible interpretation is that finite volume effects in small crystals inhibit domain rotation, although it is not clear if this is due to strong C_2 symmetry breaking, or a high density of defects that pin domain walls, or both. Similarly, Fig. 11(b) shows that the pure 180° periodic signal of sample S14K persists even into the ‘intermediate field phase’, where both S7K and sample L7K have developed additional features, including the prominent 60° signal discussed in the main body of this paper. From this we propose that the sinusoidal 60° periodic contribution to the angle-resolved torque, and by extension the presence of fluctuating zigzag order persisting beyond the boundary to the antiferromagnetically ordered phase, is an indicator of a sample with ideal stacking, although it may be that such a six-fold sinusoidal signal will appear in a 14 K sample at higher fields. We note in addition that of the 13 small samples we tested, 12 had predominantly $T_N \sim 14$ K transitions (some crystals had transitions at both 14 and 7 K), and only one had a pure 7 K transition.

We note that not only sample L7K, but also sample S7K, shows a sinusoidal six-fold signal in the intermediate field phase, of a similar size relative to the two-fold signal. This, together with the fact that the sinusoidal six-fold signal in L7K persists up to 20 K, strongly suggests that this signal is intrinsic.

Appendix C: Calibration

The cantilevers were measured in a low-temperature Wheatstone bridge configuration, via a 4-wire measurement. The measurements presented in this paper are given in volts, as measured across the Wheatstone bridge. A series of calibration measurements, with a known mass of 46 ± 1 mg solder in zero-field conditions and at 2, 20 K, was conducted to derive a conversion between volts and Nm. The mass was placed 590 ± 10 μm off-center on the cantilever to produce a twisting torque due to gravity. The calculated maximum torque for this calibration mass was $\tau = \vec{r} \times F_g = (2.66 \pm 0.07) \times 10^{-7}$ Nm. The angle resolved torque of this calibration mass was measured and the result was fit with a sin function to determine the amplitude. The conversion was measured to be 27.7 ± 0.9 Nm/V, which together with the dimensions of the sample gives a torque-density conversion factor of $(17 \pm 4) \times 10^{10}$ Nm^{-2}/V .

- [1] J. G. Rau, E. K.-H. Lee, and H.-Y. Kee, Spin-orbit physics giving rise to novel phases in correlated systems: Iridates and related materials, *Annual Review of Condensed Matter Physics* **7**, 195 (2016).
- [2] I. Rousochatzakis, N. B. Perkins, Q. Luo, and H.-Y. Kee, Beyond kitaev physics in strong spin-orbit coupled magnets, (2023), arXiv:2308.01943 [cond-mat].
- [3] W. Witczak-Krempa, G. Chen, Y. B. Kim, and L. Balents, Correlated quantum phenomena in the strong spin-orbit regime, *Annual Review of Condensed Matter Physics* **5**, 57 (2014).
- [4] T. Takayama, J. Chaloupka, A. Smerald, G. Khaliullin, and H. Takagi, Spin-orbit-entangled electronic phases in 4 d and 5 d transition-metal compounds, *Journal of the Physical Society of Japan* **90**, 062001 (2021).
- [5] A. Kitaev, Anyons in an exactly solved model and beyond, *Annals of Physics* **321**, 2 (2006).
- [6] M. Hermanns, I. Kimchi, and J. Knolle, Physics of the kitaev model: Fractionalization, dynamic correlations, and material connections, *Annual Review of Condensed Matter Physics* **9**, 17 (2018).
- [7] H. Takagi, T. Takayama, G. Jackeli, G. Khaliullin, and S. E. Nagler, Concept and realization of kitaev quantum spin liquids, *Nature Reviews Physics* **1**, 264 (2019).
- [8] Y. Motome and J. Nasu, Hunting majorana fermions in kitaev magnets, *Journal of the Physical Society of Japan* **89**, 012002 (2020).
- [9] S. M. Winter, Y. Li, H. O. Jeschke, and R. Valentí, Challenges in design of kitaev materials: Magnetic interactions from competing energy scales, *Physical Review B* **93**, 214431 (2016).
- [10] S. M. Winter, A. A. Tsirlin, M. Daghofer, J. Van Den Brink, Y. Singh, P. Gegenwart, and R. Valentí, Models and materials for generalized kitaev magnetism, *Journal of Physics: Condensed Matter* **29**, 493002 (2017).
- [11] J. G. Rau, E. K.-H. Lee, and H.-Y. Kee, Generic spin model for the honeycomb iridates beyond the kitaev limit, *Physical Review Letters* **112**, 077204 (2014).
- [12] L. Janssen, E. C. Andrade, and M. Vojta, Magnetization processes of zigzag states on the honeycomb lattice: Identifying spin models for α -rucl₃ and na₂iro₃, *Physical Review B* **96**, 064430 (2017).
- [13] J. A. Sears, L. E. Chern, S. Kim, P. J. Bereciartua, S. Francoual, Y. B. Kim, and Y.-J. Kim, Ferromagnetic kitaev interaction and the origin of large magnetic anisotropy in α -rucl₃, *Nature Physics* **16**, 837 (2020).
- [14] P. Lampen-Kelley, S. Rachel, J. Reuther, J.-Q. Yan, A. Banerjee, C. A. Bridges, H. B. Cao, S. E. Nagler, and D. Mandrus, Anisotropic susceptibilities in the honeycomb kitaev system α -rucl₃, *Physical Review B* **98**, 100403(R) (2018).
- [15] C. Balz, P. Lampen-Kelley, A. Banerjee, J. Yan, Z. Lu, X. Hu, S. M. Yadav, Y. Takano, Y. Liu, D. A. Tennant, M. D. Lumsden, D. Mandrus, and S. E. Nagler, Finite field regime for a quantum spin liquid in α -rucl₃, *Physical Review B* **100**, 060405(R) (2019).
- [16] J. A. Sears, Y. Zhao, Z. Xu, J. W. Lynn, and Y.-J. Kim, Phase diagram of α -rucl₃ in an in-plane magnetic field, *Physical Review B* **95**, 180411(R) (2017).
- [17] J. S. Gordon and H.-Y. Kee, Testing topological phase transitions in kitaev materials under in-plane magnetic fields: Application to α -rucl₃, *Physical Review Research* **3**, 013179 (2021).
- [18] K. Hwang, A. Go, J. H. Seong, T. Shibauchi, and E.-G. Moon, Identification of a kitaev quantum spin liquid by magnetic field angle dependence, *Nature Communications* **13**, 323 (2022).
- [19] O. Tanaka, Y. Mizukami, R. Harasawa, K. Hashimoto, K. Hwang, N. Kurita, H. Tanaka, S. Fujimoto, Y. Matsuda, E.-G. Moon, and T. Shibauchi, Thermodynamic evidence for a field-angle-dependent majorana gap in a kitaev spin liquid, *Nature Physics* **18**, 429 (2022).
- [20] Y. Kasahara, T. Ohnishi, Y. Mizukami, O. Tanaka, S. Ma, K. Sugii, N. Kurita, H. Tanaka, J. Nasu, Y. Motome, T. Shibauchi, and Y. Matsuda, Majorana quantization and half-integer thermal quantum hall effect in a kitaev spin liquid, *Nature* **559**, 227 (2018).
- [21] S.-H. Do, S.-Y. Park, J. Yoshitake, J. Nasu, Y. Motome, Y. S. Kwon, D. T. Adroja, D. J. Voneshen, K. Kim, T.-H. Jang, J.-H. Park, K.-Y. Choi, and S. Ji, Majorana fermions in the kitaev quantum spin system α -rucl₃, *Nature Physics* **13**, 1079 (2017).
- [22] J. A. Sears, M. Songvilay, K. W. Plumb, J. P. Clancy, Y. Qiu, Y. Zhao, D. Parshall, and Y.-J. Kim, Magnetic order in α -rucl₃: A honeycomb-lattice quantum magnet with strong spin-orbit coupling, *Physical Review B* **91**, 144420(R) (2015).
- [23] S. Widmann, V. Tsurkan, D. A. Prishchenko, V. G. Mazurenko, A. A. Tsirlin, and A. Loidl, Thermodynamic evidence of fractionalized excitations in α -rucl₃, *Physical Review B* **99**, 094415 (2019).
- [24] J. A. N. Bruin, R. R. Claus, Y. Matsumoto, N. Kurita, H. Tanaka, and H. Takagi, Robustness of the thermal hall effect close to half-quantization in α -rucl₃, *Nature Physics* **18**, 401 (2022).
- [25] Y. Kasahara, S. Suetsugu, T. Asaba, S. Kasahara, T. Shibauchi, N. Kurita, H. Tanaka, and Y. Matsuda, Quantized and unquantized thermal hall conductance of the kitaev spin liquid candidate α -rucl₃, *Physical Review B* **106**, L060410 (2022).
- [26] E. Lefrançois, G. Grissonnanche, J. Baglo, P. Lampen-Kelley, J.-Q. Yan, C. Balz, D. Mandrus, S. E. Nagler, S. Kim, Y.-J. Kim, N. Doiron-Leyraud, and L. Taillefer, Evidence of a phonon hall effect in the kitaev spin liquid candidate α -rucl₃, *Physical Review X* **12**, 021025 (2022).
- [27] P. Czajka, T. Gao, M. Hirschberger, P. Lampen-Kelley, A. Banerjee, N. Quirk, D. G. Mandrus, S. E. Nagler, and N. P. Ong, Planar thermal hall effect of topological bosons in the kitaev magnet α -rucl₃, *Nature Materials* **22**, 36 (2023).
- [28] K. A. Modic, M. D. Bachmann, B. J. Ramshaw, F. Arnold, K. R. Shirer, A. Estry, J. B. Betts, N. J. Ghimire, E. D. Bauer, M. Schmidt, M. Baenitz, E. Svanidze, R. D. McDonald, A. Shekhter, and P. J. W. Moll, Resonant torsion magnetometry in anisotropic quantum materials, *Nature Communications* **9**, 3975 (2018).
- [29] K. A. Modic, R. D. McDonald, J. P. C. Ruff, M. D. Bachmann, Y. Lai, J. C. Palmstrom, D. Graf, M. K. Chan, F. F. Balakirev, J. B. Betts, G. S. Boebinger, M. Schmidt, M. J. Lawler, D. A. Sokolov, P. J. W. Moll, B. J. Ramshaw, and A. Shekhter, Scale-invariant mag-

- netic anisotropy in rucl_3 at high magnetic fields, *Nature Physics* **17**, 240 (2021).
- [30] K. Riedl, Y. Li, S. M. Winter, and R. Valentí, Sawtooth torque in anisotropic $j_{eff} = 1/2$ magnets: Application to $\alpha\text{-rucl}_3$, *Physical Review Letters* **122**, 197202 (2019).
- [31] I. A. Leahy, C. A. Pocs, P. E. Siegfried, D. Graf, S.-H. Do, K.-Y. Choi, B. Normand, and M. Lee, Anomalous thermal conductivity and magnetic torque response in the honeycomb magnet $\alpha\text{-rucl}_3$, *Physical Review Letters* **118**, 187203 (2017).
- [32] B. W. Lebert, S. Kim, D. A. Prishchenko, A. A. Tsirlin, A. H. Said, A. Alatas, and Y.-J. Kim, Acoustic phonon dispersion of $\alpha\text{-rucl}_3$, *Phys. Rev. B* **106**, L041102 (2022).
- [33] C. Balz, L. Janssen, P. Lampen-Kelley, A. Banerjee, Y. H. Liu, J.-Q. Yan, D. G. Mandrus, M. Vojta, and S. E. Nagler, Field-induced intermediate ordered phase and anisotropic interlayer interactions in $\alpha\text{-rucl}_3$, *Physical Review B* **103**, 174417 (2021).
- [34] A. Banerjee, P. Lampen-Kelley, J. Knolle, C. Balz, A. A. Aczel, B. Winn, Y. Liu, D. Pajerowski, J. Yan, C. A. Bridges, A. T. Savici, B. C. Chakoumakos, M. D. Lumsden, D. A. Tennant, R. Moessner, D. G. Mandrus, and S. E. Nagler, Excitations in the field-induced quantum spin liquid state of $\alpha\text{-rucl}_3$, *npj Quantum Materials* **3**, 8 (2018).
- [35] J. Wagner, A. Sahasrabudhe, R. B. Versteeg, L. Wysocki, Z. Wang, V. Tsurkan, A. Loidl, D. I. Khomskii, H. Hedayat, and P. H. M. van Loosdrecht, Magneto-optical study of metamagnetic transitions in the antiferromagnetic phase of $\alpha\text{-rucl}_3$, *npj Quantum Materials* **7**, 28 (2022).
- [36] R. D. Johnson, S. C. Williams, A. A. Haghighirad, J. Singleton, V. Zapf, P. Manuel, I. I. Mazin, Y. Li, H. O. Jeschke, R. Valentí, and R. Coldea, Monoclinic crystal structure of $\alpha\text{-rucl}_3$ and the zigzag antiferromagnetic ground state, *Physical Review B* **92**, 235119 (2015).
- [37] S. Kim, E. Horsley, J. P. C. Ruff, B. D. Moreno, and Y.-J. Kim, Structural transition and magnetic anisotropy in $\alpha\text{-rucl}_3$, (2023), arXiv:2311.04000 [cond-mat].
- [38] S.-Y. Park, S.-H. Do, K.-Y. Choi, D. Jang, T.-H. Jang, J. Schefer, C.-M. Wu, J. S. Gardner, J. M. S. Park, J.-H. Park, and J. S., Emergence of the isotropic kitaev honeycomb lattice with two-dimensional ising universality in $\alpha\text{-rucl}_3$, arXiv:1609.05690 [cond-mat].
- [39] A. Banerjee, J. Yan, J. Knolle, C. A. Bridges, M. B. Stone, M. D. Lumsden, D. G. Mandrus, D. A. Tennant, R. Moessner, and S. E. Nagler, Neutron scattering in the proximate quantum spin liquid $\alpha\text{-rucl}_3$, *Science* **356**, 1055 (2017).
- [40] H. B. Cao, A. Banerjee, J.-Q. Yan, C. A. Bridges, M. D. Lumsden, D. G. Mandrus, D. A. Tennant, B. C. Chakoumakos, and S. E. Nagler, Low-temperature crystal and magnetic structure of $\alpha\text{-rucl}_3$, *Physical Review B* **93**, 134423 (2016).
- [41] S. Kim, B. Yuan, and Y.-J. Kim, $\alpha\text{-rucl}_3$ and other kitaev materials, *Applied Physics Letters Materials* **10**, 080903 (2022).